ELSEVIER

0267-7261(94)00036-0

Soil Dynamics and Earthquake Engineering 14 (1995) 103–114

0267-7261/95/$09.50

Seismological evidence for nonlinear elastic ground behavior during large earthquakes

Igor A. Beresnev, Kuo-Liang Wen & Yeong Tein Yeh

Institute of Earth Sciences, Academia Sinica, P.O. Box 1-55, Nankang, Taipei 11529, Taiwan

(Received 24 February 1994; revised version received 20 July 1994; accepted 22 July 1994)

Amplification of earthquake-induced seismic waves by soft superficial deposits often causes significant damages in the urban areas. In predicting this effect for large future earthquakes, the linear elastic response of soils is customarily assumed. To check this assumption, we have analyzed surface and downhole acceleration data from the SMART1 and SMART2 strong motion arrays in Taiwan, covering peak accelerations of up to 0·3 g. First, frequency-dependent amplification induced by the alluvial deposits at the SMART1 array was estimated using spectral ratio technique, where the records at rock site were taken as a reference motion. Statistically validated reduction in soil amplification in the strong motion relative to the weak motion in the frequency range between approximately 1 and 9 Hz was detected. Secondly, relative site responses between the Pleistocene and recent sedimentary deposits at the SMART2 array were studied. Relative amplification was shown to be clearly dependent on the excitation level. Thirdly, we compared experimentally recorded uphole/downhole spectral ratios on weak and strong ground motion with the theoretical response yielded by the geotechnical code DESRA2 which assumes hysteretic constitutive relationship of soil. Major symptoms of nonlinear ground behavior predicted by the model were found in the observed data. Back-calculation of the shear wave velocities to the depth of 47 m shows nearly 50% decrease in the strongest quakes, also accounted for by the nonlinear soil behavior.

Key words: strong motion, soil amplification, shear wave velocity, nonlinear deformation, elastic hysteresis.

1 INTRODUCTION

It has long been understood that seismic waves generated by earthquakes are magnified by low-impedance superficial deposits.[1,2] Among the most dramatic recent demonstrations of this effect were the 1985 Michoacan (Mexico) Earthquake and the 1989 Loma Prieta (California) Earthquake, where the extent of damage from soil amplification was catastrophic in Mexico City[3,4] and significant in the areas of San Francisco and Oakland.[5]

Nearly all of the ground motion prediction models employed in seismology assume the linear elastic behavior of the ground during earthquakes; as a result, soil amplification correction is introduced by a mere multiplication of the synthetic seismogram by the corresponding amplification factor.[6–8] These factors are usually empirically deduced from the records of weak seismic events, microtremors, or coda waves.[9,10] It is believed that there is no significant difference in the soil amplification on weak and strong motion.

However, the above commonplace seismological practice is in contradiction with the concept of ground deformation largely adopted in geotechnical engineering, where the dynamics of the structures substantially influenced by the local behavior of the ground is of great concern. On the basis of the results of the cycling loading tests performed on soil samples, geotechnical engineers have recognized that shear deformation in soil deviates from the linear elasticity above a certain threshold acceleration.[11–16] Accordingly, nonlinear site effects have been taken into account in earthquake engineering in modelling soil response to seismic loading.[10] This contradiction has not been resolved hitherto and has remained a subject of continuous debate.[10,17–20] Seismologists are reluctant to accept nonlinear ground response basically because of the lack of compelling evidence of nonlinear effects

appearing in the realistically observed free-field strong motion accelerograms.

Simultaneous observation of weak and sufficiently intensive ground motion having PGA (peak ground acceleration) larger than 0·2–0·3 g ($g \approx 980\,\mathrm{cm/s^2}$) at a group of seismic stations has been a rarity in seismology. Yet, only beyond this conjectural acceleration level can appreciable nonlinear effects be expected from the geotechnical calculations.[11,21–22] A large amount of digital strong motion data has been made available recently since the deployment of dense, continually operating strong motion arrays in California, Japan, Taiwan and other places. This has yielded an opportunity to quantitatively study the *in-situ* nonlinear soil response characteristics. In this paper, we address the local earthquake data recorded by the SMART1 and SMART2 arrays in Taiwan which have been in successive non-stop operation since 1980.[23,24] Peak accelerations recorded to date reach approximately 0.3 g. We focus on the nonlinear effects such as the reduction in shear wave velocity and the increase in soil damping, occurring in the near-surface deposits as the excitation strength changes from low to high. A clear manifestation of the nonlinear phenomena is seismologically detected for the surface accelerations surpassing roughly 0·15–0·2 g.

In this investigation, we undertake a systematic examination of the nonlinear site effects using a large ensemble of weak and strong motion records obtained on surface and in boreholes. The problem of understanding the physics of ground deformation at the damaging acceleration level is of great practical importance. Our findings show that nonlinear seismic effects may play a more fundamental role than seismologists used to think.

2 WHAT DO WE CALL THE NONLINEAR SITE EFFECT IN SEISMIC MOTION?

The basic concept of nonlinear soil behavior comes from the vibratory tests on soil samples performed under laboratory conditions, which show that soil shearing deformation follows the hysteretic law.[15,25] A typical stress–strain relationship in soft soil, adapted from Ref. 26, is sketched in Fig. 1. Initial loading curve has a hyperbolic form (broken line). Subsequent unloading and reloading phases track a hysteretic path.

Once the hysteretic form of a constitutive law is postulated, two corollaries for observational seismology follow. Firstly, the shear modulus, which is defined by the angle between the stress–strain curve and the horizontal axis, takes its maximum value G_{max} at the origin, i.e. in the infinitesimal deformation. At the finite deformation, the effective secant modulus G_{sec}, defined by the slope of the line connecting the initial point and the turning corner of the hysteresis loop, is always

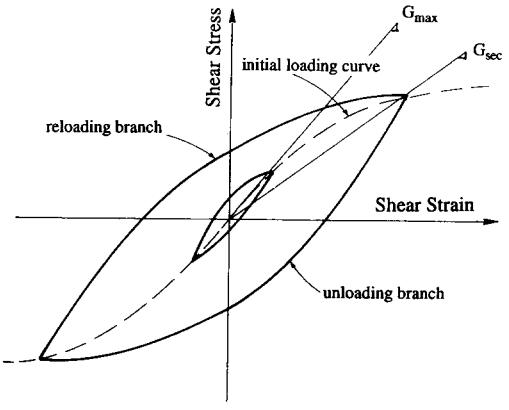

Fig. 1. Typical stress–strain relationships of soil in shear deformation.

lower. Since the shear wave velocity V is related to the shear modulus by the formula $V = \sqrt{G/\rho}$, where ρ is the density, V is always reduced as the strain amplitude increases. Assuming a simple 1D geological structure with one soil layer over a half-space, this effect will result in a shift of the resonance frequencies of the layer to the lower values with increasing excitation amplitude, which should be observed from the spectra of the recorded ground motion. Indeed, since the resonances occur at the frequencies proportional to the fundamental frequency $f = V/4H$, where H is the layer thickness,[1] reduction in V is associated with the reduction in f.

Secondly, the finite area of the hysteresis loop implies a loss of energy in each deformation cycle, which induces a specific hysteretic damping becoming more significant as the strain level increases. Laboratory data show that hysteretic damping in soils is frequency-independent.[25] In summarizing, observational seismologists dealing with the free-field strong motion seismograms should see the symptoms of nonlinear site effect in the reduction of observed velocities and the lowering of soil amplification functions, both happening as the amplitude of shaking increases.

3 EXISTING EVIDENCE OF NONLINEAR SOIL RESPONSE

Unambiguous observations of nonlinear site effects in strong ground motion have been scarce. However, Tokimatsu and Midorikawa[27] did demonstrate a shear modulus degradation effect from a limited number of strong motion accelerograms at several sedimentary sites in Japan. Additionally, Chang *et al.*[28] reported a shear wave velocity reduction derived from the accelerograms of two events recorded by the LSST (Lotung large-scale seismic test program) downhole array in Taiwan.

Rather contradictory results on the deamplification phenomena observed by surface stations during the recent large Coalinga, Michoacan and Loma Prieta earthquakes were reported in Refs 18 and 29–32 (the

term 'deamplification' is commonly used to refer to the nonlinear effect of the reduction in soil amplification in the strong ground motion compared to the weak motion). In Ref. 29, the peak accelerations of up to 0·7 g were addressed, and the soil response was found to be essentially linear except for the narrow frequency band from 10–11 Hz. Refs 30 and 31 simultaneously reported linear and nonlinear ground responses in Mexico City during the destructive Michoacan earthquake. The problem of nonlinear seismic response was in the spotlight again when considerable discrepancy between the strong and weak motion amplification factors was reported by Chin and Aki[18] for the epicentral zone of the Loma Prieta Earthquake; however, Darragh and Shakal[32] reported mixed results during the same earthquake. Despite somewhat discrepant observations, the Loma Prieta Earthquake was the one after which the importance of the nonlinear seismic phenomena began to be actively discussed in the seismological community.

4 SMART1 AND SMART2 STRONG MOTION ARRAYS

The SMART1 accelerograph array was installed in the north-east corner of Taiwan[23] (Fig. 2). It comprises 39 force-balanced triaxial accelerometers configured in three concentric circles. There is one station C-00 at the centre. All the stations are installed on the recent alluvial plain with uniform soft soil conditions. One station (E-02) is positioned outside the outer ring on the slate outcrop and is classified as a hard rock station.

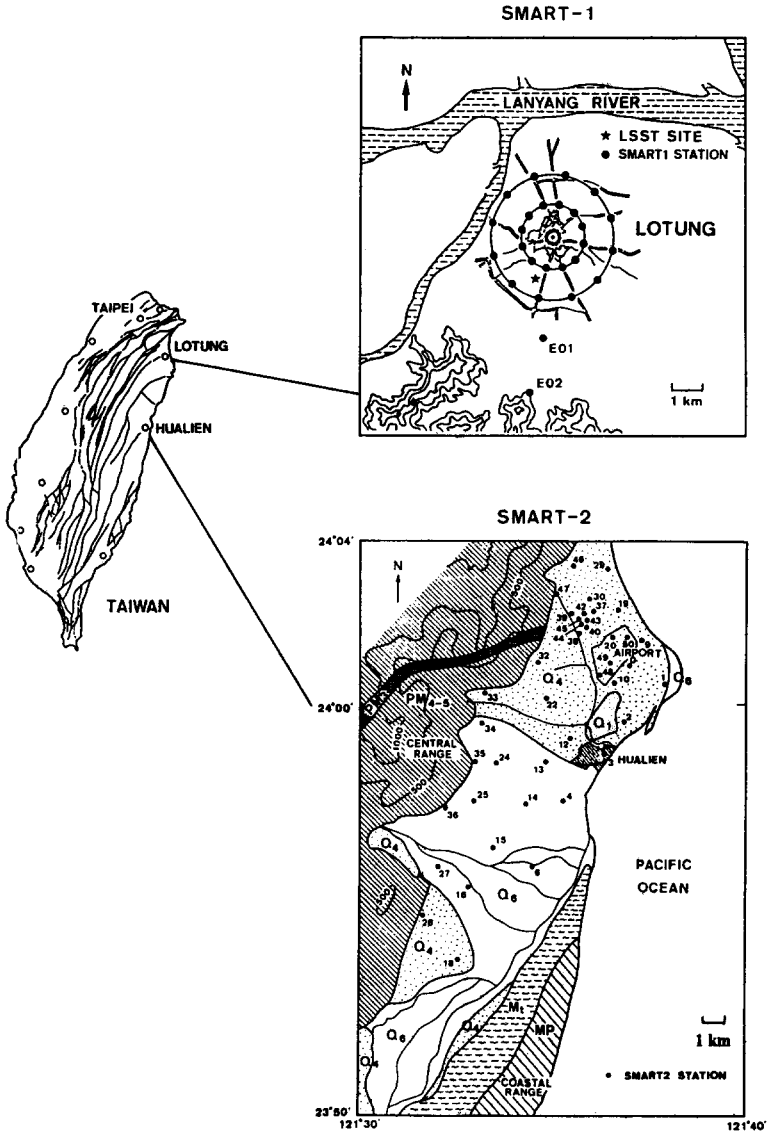

Fig. 2. Location and layout of the SMART1 and SMART2 arrays. Q_6 is the recent alluvium, Q_4 is Pleistocene terrace deposits (gravel, sand, clay), Q_1 is Pleistocene mudstone, siltstone, sandstone, gravel; MP is late-Miocene to Pliocene conglomerate, shale, siltstone, sandstone; Mt is early Miocene agglomerate and tuffaceous sandstone; PM_{4-5} is late Paleozoic to Mesozoic schist, and PM_3 is late Paleozoic to Mesozoic limestone.

SMART1 ground motions are digitized as 12-bit words at 100 samples/s.

A vertical accelerograph array has been installed in the borehole drilled to a depth of 47 m in the alluvial deposits in the south-west quadrant of the SMART1 array (LSST site, Fig. 2). A shear wave velocity structure in the borehole obtained by the uphole and crosshole shooting methods and corresponding to small-deformation waves is shown in Fig. 3. Accelerographs were placed at the surface and at the depths of 6, 11, 17 and 47 m, and digital data were recorded as 12-bit words at 200 samples/s.

The SMART2 accelerograph array is currently deployed on the eastern coast of Taiwan (Fig. 2). It consists of about 45 surface stations dispersed over the area of roughly 20×10 km. All of the stations are located in the sedimentary valley bordering upon the Central Range in the west and the Coastal Range or the Pacific coast in the east. Stations are either on Pleistocene terrace deposits or recent alluvium. The borehole drilled near station 37 through the terrace deposits to a depth of 200 m disclosed a gradual increase in the shear wave velocity from approximately 100 to 1060 m/s.[33] All SMART2 stations are equipped with Kinemetrics FBA-23 16-bit three-component accelerometers and the SSR-1 recorders. The sampling rate is 200 words/s.

5 OBSERVED DIFFERENCES IN WEAK AND STRONG MOTION AMPLIFICATION

5.1 Method of amplification function calculation

To assess the site amplification function, the spectral ratio method in which the Fourier amplitude spectrum of acceleration at soil station is divided by the spectrum at rock reference station is employed. Station E-02 is used as a reference site in the SMART1 data analysis. Spectral ratios are calculated as follows: (1) an 8-s window containing the shear wave is identified, (2) the window is tapered on both sides using a 5%-of-window-length half-bell cosine function, (3) the Fourier amplitude spectrum is calculated; (4) the spectrum is smoothed using a 3-point running Hanning mean filter; (5) the ratio of two smoothed spectra is calculated; (6) the ratio is corrected for differential attenuation and geometric spreading effects using the formula[29]

$$\frac{S_1}{S_2} = \frac{g_1}{g_2}\frac{r_1}{r_2} e^{\pi(r_1 - r_2)f/VQ}, \quad (1)$$

where S_1/S_2 is the 'true' site response, g_i is the spectrum of the recorded ground motion, r_i is the hypocentral distance, f is the frequency, V is the shear wave velocity, and Q is the quality factor. In the calculations we assumed $V = 3{\cdot}5$ km/s and $Q = 225f^{1{\cdot}1}$ which is characteristic for north-east Taiwan.[34] The choice of V and Q affects the spectral ratio estimates. We varied V between 3·0 and 4·0 km/s and Q between $Q = 225f^{1{\cdot}1}$ and $Q = 125f^{0{\cdot}79}$ (Ref. 34). The two extreme expressions for Q correspond to the decrease and increase of the attenuation coefficient with frequency, respectively. The maximum differences in spectral ratios produced by these variations for the spacing between stations equal to 10 km are 4% at 1 Hz, 10% at 10 Hz, and 15% at 30 Hz. Strictly speaking, the above Q-values are valid up to the frequencies of 10 Hz only. We extrapolated them to 30 Hz which may not be precisely correct.

We are concerned with only the horizontal components of acceleration in this study. Correspondingly, the mean 'horizontal' spectral ratios will be shown, which are calculated by summing the squares of the ratios for the EW- and NS-components, dividing by two, and taking the square root. The noise level in the accelerogram is always assessed by dividing the smoothed amplitude spectrum of the S-wave window by the spectrum of the pre-event noise. The spectral ratios are plotted only in the frequency bands where the signal-to-noise proportion is greater than five.

5.2 Soil amplification on SMART1 array

Figure 4 shows the frequency-dependent site amplification functions of the SMART1 central station C-00, calculated on weak and strong motion. The average

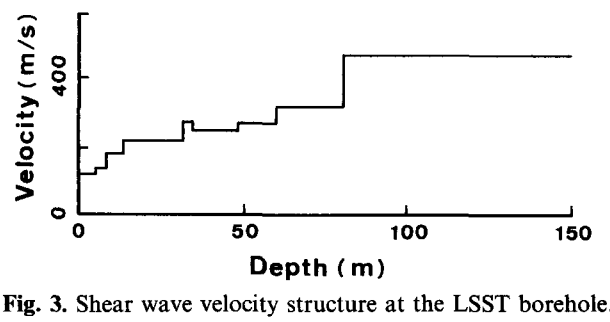

Fig. 3. Shear wave velocity structure at the LSST borehole.

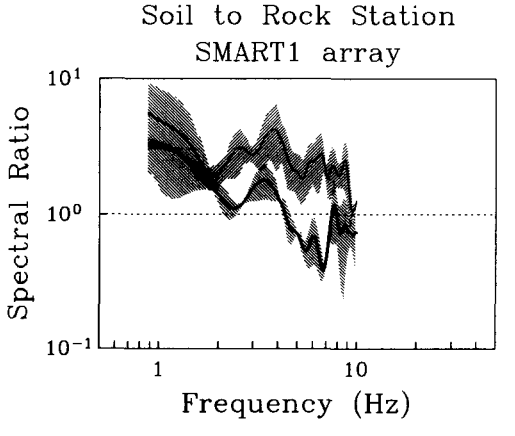

Fig. 4. Average amplification functions of the alluvial deposits under the central station of the SMART1 array on weak and strong motion (thin and thick line, respectively).

Table 1. Selected SMART1 events

Event no. and date	Peak acceler. C-00/Peak acceler. E-02 (cm/s^2) EW	NS	M_L	Depth (km)	Δ^a(C-00)/Δ(E-02) (km)
		Weak motions			
25 (21/09/83)	27·8/19·6	28·0/19·8	6·8	18·0	100·5/96·9
32 (12/06/85)	19·5/6·1	17·9/13·5	6·0	5·3	48·5/48·2
34 (05/08/85)	17·6/15·4	20·9/12·1	5·8	1·3	34·4/30·1
		Strong motions			
39 (16/01/86)	212·2/166·2	266·7/197·5	6·5	10·2	24·4/27·0
40 (20/05/86)	170·3/185·9	228·9/95·9	6·6	15·8	69·7/65·1
45 (14/11/86)	120·4/133·2	150·5/139·8	7·0	13·9	77·3/72·7
		Aftershock and coda			
40 coda[b]	35·7/12·0	32·8/13·1			
41 (20/05/86)	35·8/32·5	50·6/49·1	6·2	21·8	74·2/69·6

[a]Hypocentral distance to the station in parenthesis.
[b]Eight-seconds-long coda window starting at 8 s after S-wave arrival.

curves calculated over the ensembles of three weak and three strong events are shown; the hatched bands represent ±1 standard deviation around the average. Stations C-00 and E-02 are 4·8 km apart. Parameters of the events used in calculation are summarized in Table 1.

Quantification of the events on 'weak' and 'strong' is done according to the PGA achieved. In the SMART1 data, the events with horizontal PGA less than 30 cm/s^2 and larger than 100 cm/s^2 are attributed to the weak and strong motion classes, respectively. The largest horizontal acceleration in the records is 267 cm/s^2. The events for which the curves in Fig. 4 are calculated were chosen to be relatively distant from the stations in order to reduce the contamination of the spectral ratios by the differential source and path effects. The minimum hypocentral distance is 24·4 km as seen in Table 1, and the local magnitude of the events ranges from 5·8 to 7·0. The error in the amplification function estimate is supposed to be included in the value of standard deviation.

Figure 4 shows that the alluvium site amplifies the weak motion at all frequencies. On the other hand, the strong motion ratio lies below the weak motion curve between approximately 2 and 9 Hz, the departure being much larger than the error margin. The differences between weak and strong motion spectral ratios most probably indicate that nonlinear deamplification at the soil site took place. Strong motion amplification drops below the unity between 4·5 and 7·5 Hz, turning it into damping. Maximum deamplification occurs near 6·5 Hz where the average weak motion amplification is 2·9 compared with only 0·40 in the strong motion. This observation shows that the ability of soil to amplify upcoming seismic waves may be completely lost when the amplitude of motion becomes sufficiently strong.

Figure 5 presents the individual weak and strong motion spectral ratios for the same pair of stations calculated for the M_L 6·6 earthquake of 20 May 1986 (event 40 in Table 1), its aftershock (event 41) and its shear wave coda. Aftershock occurred approximately 11 min after the main shock and had a close hypocentre. The PGAs in the main shock, aftershock and coda are 229, 51 and 36 cm/s^2, respectively. The minimum hypocentral distance is 65·1 km, making the differential source and path effect contributions to the spectral ratios insignificant. Eight-seconds-long realization of coda immediately following shear wave window was used. Corresponding waveforms are depicted in Fig. 6. It is seen that the window length of 8 s is long enough to cover the main energy of shear waves in all instances.

Figure 5 demonstrates that both weak motion amplification functions derived after the aftershock and coda are relatively close to each other. On the other hand, the strong motion is considerably deamplified between approximately 1 and 7 Hz. Effect of the downward shift in the resonance frequency with increasing quake amplitude is also clearly seen if the ratios of the main shock and coda are compared, where the clearest resonance shifts from approximately 4·5 to 3·5 Hz. However, the resonance frequency in the aftershock is only slightly higher than in the main shock.

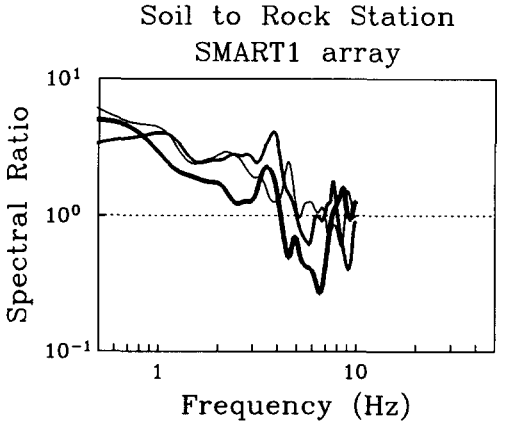

Fig. 5. Amplification functions at C-00 site for the 20 May 1986 earthquake, its aftershock and the main shock coda (thick, half-thick and thin line, respectively).

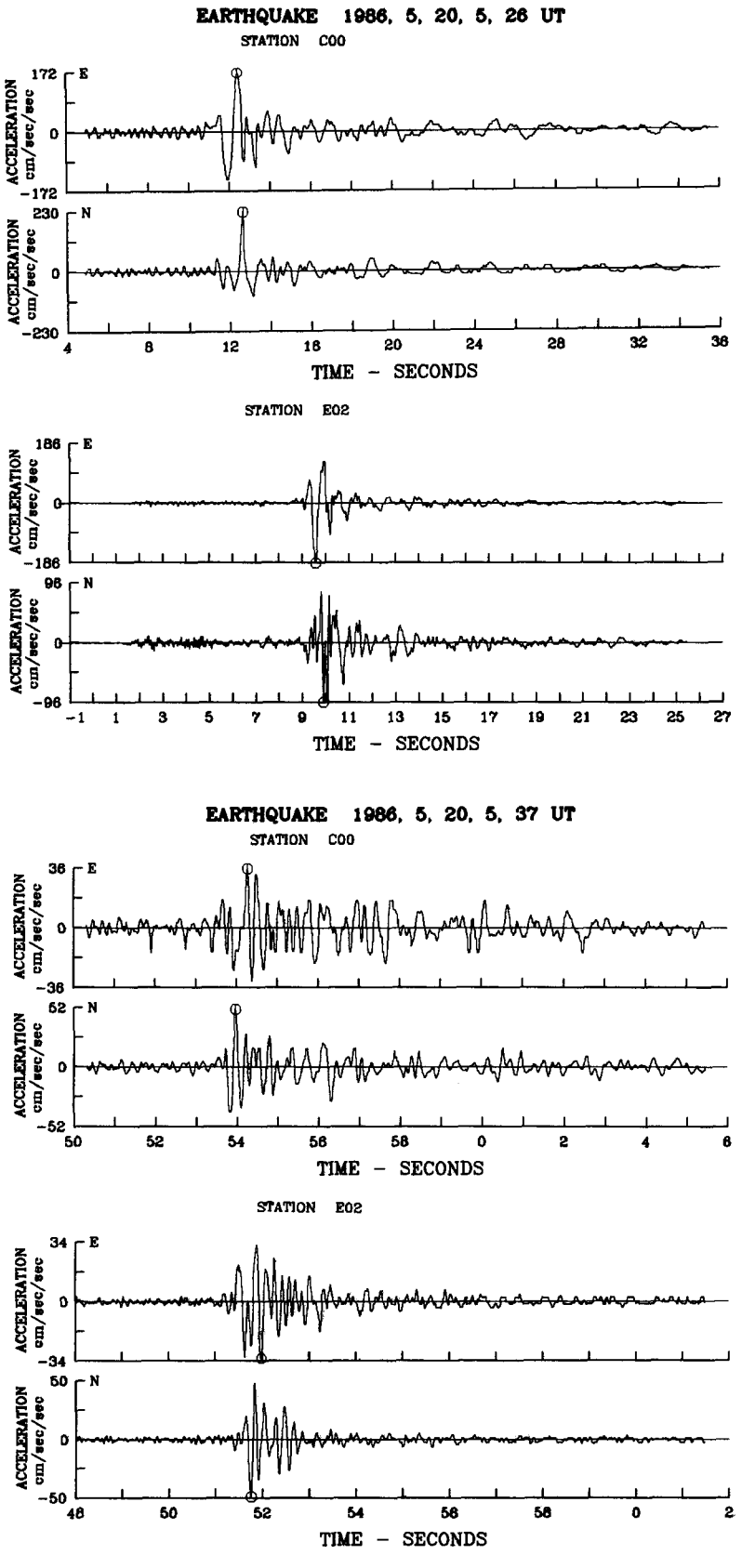

Fig. 6. Accelerograms of the earthquakes 40 and 41 of 20 May 1986 for which spectral ratios in Fig. 5 are calculated.

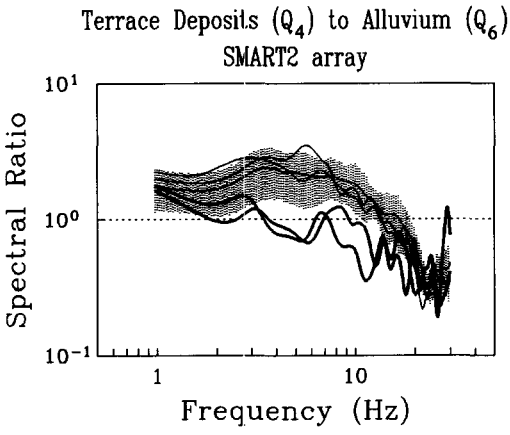

Fig. 7. Spectral ratios between stations 3 and 36 of the SMART2 array. Ratios are shown for weak (thin lines) and strong (thick lines) excitation strengths.

Figures 4 and 5 illustrate the clear nonlinear site response which occurred at the C-00 alluvial site. However, we have not addressed the records of the other soil stations of the SMART1 array assuming that they had very similar site conditions and would therefore have exhibited the same behaviour. This can be checked in the further studies.

5.3 Soil amplification on SMART2 array

In the SMART2 area, a hard rock reference station is not available, making the isolation of a genuine site response a difficult task. We focus, therefore, on the relative site effect characterized by the spectral ratios between Pleistocene terrace deposits and recent alluvium. The maximum acceleration allowed in 'weak motion' has been diminished to 13 cm/s^2, whereas the minimum acceleration for 'strong motion' remained equal to 100 cm/s^2. Because the quality of the SMART2 data has been significantly improved by using the 16-bit instruments, it allowed to considerably lower the triggering level and to record therefore a much higher number of weak events.

Figure 7 depicts spectral ratios between stations 3 and 36 of the SMART2 array on the weak and strong motion. The distance between stations is 8·4 km. Strong motion spectral ratios correspond to the earthquakes of 21 March 1992 (M_L 4.9) and 25 June 1992 (M_L 5·0) that

Table 2. Selected SMART2 events

Event no. and date	Peak acceler. 36/Peak acceler. 3 (cm/s^2) EW	NS	M_L	Depth (km)	$\Delta^a(36)/\Delta(3)$ (km)
		Weak motions			
56 (14/01/91)	6·8/7·7	3·4/11·4	4·0	0·9	16·7/11·9
59 (18/01/91)	7·5/9·5	9·4/11·0	5·2	0·9	38·0/45·3
60 (18/01/91)	4·7/10·6	4·6/5·4	4·8	3·3	38·9/46·8
62 (19/01/91)	6·7/3·5	5·5/4·2	3·7	12·6	14·6/20·0
63 (19/01/91)	2·8/4·4	4·0/5·1	5·2	5·6	29·8/32·0
64 (19/01/91)	2·3/4·6	3·8/5·4	5·0	2·3	28·1/29·7
66 (20/01/91)	3·6/3·8	4·6/5·2	3·6	8·8	11·1/17·2
67 (21/01/91)	4·4/3·7	4·6/3·4	5·0	2·6	39·0/45·7
69 (21/01/91)	8·8/8·3	12·2/7·0	5·3	2·9	38·9/45·2
103 (09/06/91)	7·7/4·9	7·3/6·9	4·3	10·7	13·4/19·4
110 (12/07/91)	10·3/5·7	12·3/8·2	4·0	10·1	13·1/19·0
113 (05/08/91)	5·7/5·0	8·5/5·9	3·7	13·5	16·8/21·0
117 (27/08/91)	5·1/8·1	5·5/8·2	4·4	7·4	28·3/25·1
118 (27/08/91)	3·0/4·3	4·9/6·7	4·2	13·3	29·4/22·5
122 (21/09/91)	4·1/5·8	4·8/8·7	4·4	12·5	30·1/23·1
126 (08/10/91)	4·6/10·6	4·0/9·8	4·5	16·3	30·2/25·5
128 (14/10/91)	4·4/7·5	5·2/11·3	4·1	8·8	19·0/12·8
129 (15/10/91)	6·4/4·5	5·6/4·4	3·7	10·1	11·8/17·7
149 (11/01/92)	4·6/4·0	3·1/4·2	4·1	34·3	41·2/37·2
151 (29/01/92)	11·0/9·1	8·7/11·1	3·5	16·1	16·2/18·5
157 (09/03/92)	4·4/4·9	4·4/4·0	4·3	22·3	26·1/23·1
159 (11/03/92)	7·3/4·3	5·9/4·7	3·3	12·6	13·8/13·6
189 (23/07/92)	11·5/11·1	12·9/11·7	4·7	21·2	24·9/26·8
193 (17/08/92)	12·5/8·1	12·5/11·0	4·3	22·6	25·2/26·9
		Strong motions			
161 (21/03/92)	219·9/152·5	220·0/295·3	4·9	22·6	24·6/24·0
183 (25/06/92)	203·9/130·1	122·4/175·3	5·0	23·4	26·1/23·6
		Coda			
161 coda[b]	16·2/31·8	12·3/26·3			
161 coda[c]	4·8/8·2	5·7/13·5			

[a]Hypocentral distance to the station in parenthesis.
[b]Eight-seconds-long coda window starting at 4 s after S-wave arrival.
[c]Eight-seconds-long coda window starting at 8 s after S-wave-arrival.

occurred almost directly beneath the array at the depths of 22·6 and 23·4 km, respectively. The horizontal PGAs produced were 295 and 204 cm/s^2, respectively. Among the three weak motion amplification functions plotted, one is the average over the ensemble of 24 small earthquakes covering a variety of azimuths, depths and epicentral distances, with the shaded area indicating the standard deviation. The two others are calculated from the coda of the earthquake of 21 March 1992 in the time windows starting at 4 and 8 s after the S-wave arrival, where the peak horizontal accelerations are 32 and 14 cm/s^2, respectively. Parameters of all earthquakes are tabulated in Table 2.

It can be seen, first of all, that the coda ratios are statistically indistinguishable from the average curve obtained from the 24 independent earthquakes. This result is evidence that a single amplification function obtained from the S-wave coda is equivalent to the mean weak motion amplification obtained from a representative number of small earthquakes. Secondly, the strong motion spectral ratios closely follow each other and are appreciably reduced compared with those in weak motion in the frequency range of approximately 3–14 Hz. The apparent 'deamplification' effect is well in excess of the uncertainty imposed by the standard deviations and can be accounted for by the differential nonlinear behaviour of soils underlying these two recording sites.

Since the curves in Fig. 7 represent the relative response of two soil sites, the 'deamplification' in this case merely shows that terrace deposits exhibit a larger damping at high strains than the alluvial sediments. In this sense, the alluvial deposits behave as a more rigid substratum in spite of their younger age, which seems paradoxical at first glance. However, this effect is real. To check it, we similarly calculated the relative Q_4/Q_6 responses on weak and strong motion for the other SMART2 station pairs 19 and 35, 20 and 15, and 33 and 15 which have an interstation distances varying from 7·9 to 11·4 km and the differences in the spatial alignment of up to 79°. In all these instances, the Q_4/Q_6 ratio has always been reduced in strong motion compared to weak motion between approximately 1 and 10 Hz.

5.4 Soil amplification derived from downhole data of LSST array

A very reliable way to estimate the true soil response is to take the spectral ratio between uphole and downhole instruments, when appropriate borehole acceleration data are available. Nonlinear site response in the upward vertically-propagating transverse wave has recently been modelled in Ref. 19 using public-domain geotechnical computer code DESRA2[35] which postulated hysteresis-type constitutive law. Figure 8(a), reproduced from Ref. 19, shows the computed spectral

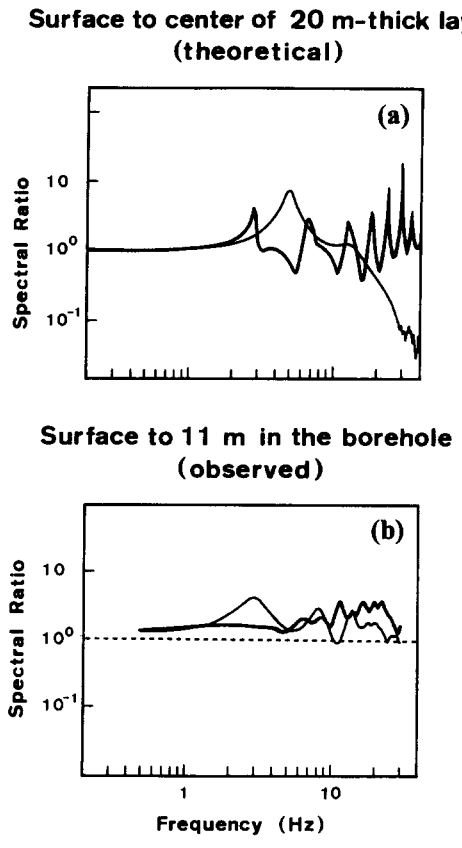

Fig. 8. (a) Theoretical spectral ratios of accelerations at the surface to the centre of a soil layer in linear and nonlinear responses (thin and thick line, respectively) (after Ref. 19). (b) Experimentally recorded ratios between the surface and the depth of 11 m at the LSST array in the strong shock (thick line) and the aftershock (thin line).

Table 3. Selected LSST events

Event no. and date	Depth (km)	M_L	Δ^a (km)	PGA at surface (cm/s^2)
3 (07/11/85)	74	5·5	17	27·3
4 (16/01/86)	10	6·5	24	258·0
5 (29/03/86)	10	4·7	8	41·4
6 (08/04/86)	11	5·4	31	35·4
7 (20/05/86)	16	6·6	66	223·6
8 (20/05/86)	22	6·2	69	35·0
9 (11/07/86)	1	4·5	5	72·8
10 (16/07/86)	1	4·5	6	70·0
11 (17/07/86)	2	5·0	6	118·6
12 (30/07/86)	2	6·2	5	186·7
14 (30/07/86)	2	4·9	5	57·5
15 (05/08/86)	1	4·9	5	98·0
16 (14/11/86)	7	7·0	78	167·2
19 (08/12/86)	27	5·8	45	48·0
20 (10/12/86)	98	5·8	42	23·8
21 (06/01/87)	28	6·2	77	31·8
22 (04/02/87)	70	5·8	16	43·4
23 (24/06/87)	31	5·7	52	31·7
24 (27/06/87)	1	5·3	40	23·7
25 (10/11/87)	34	5·2	27	79·2
26 (19/08/88)	91	5·9	96	22·4
27 (18/09/88)	63	5·6	68	22·3

[a]Epicentral distance.

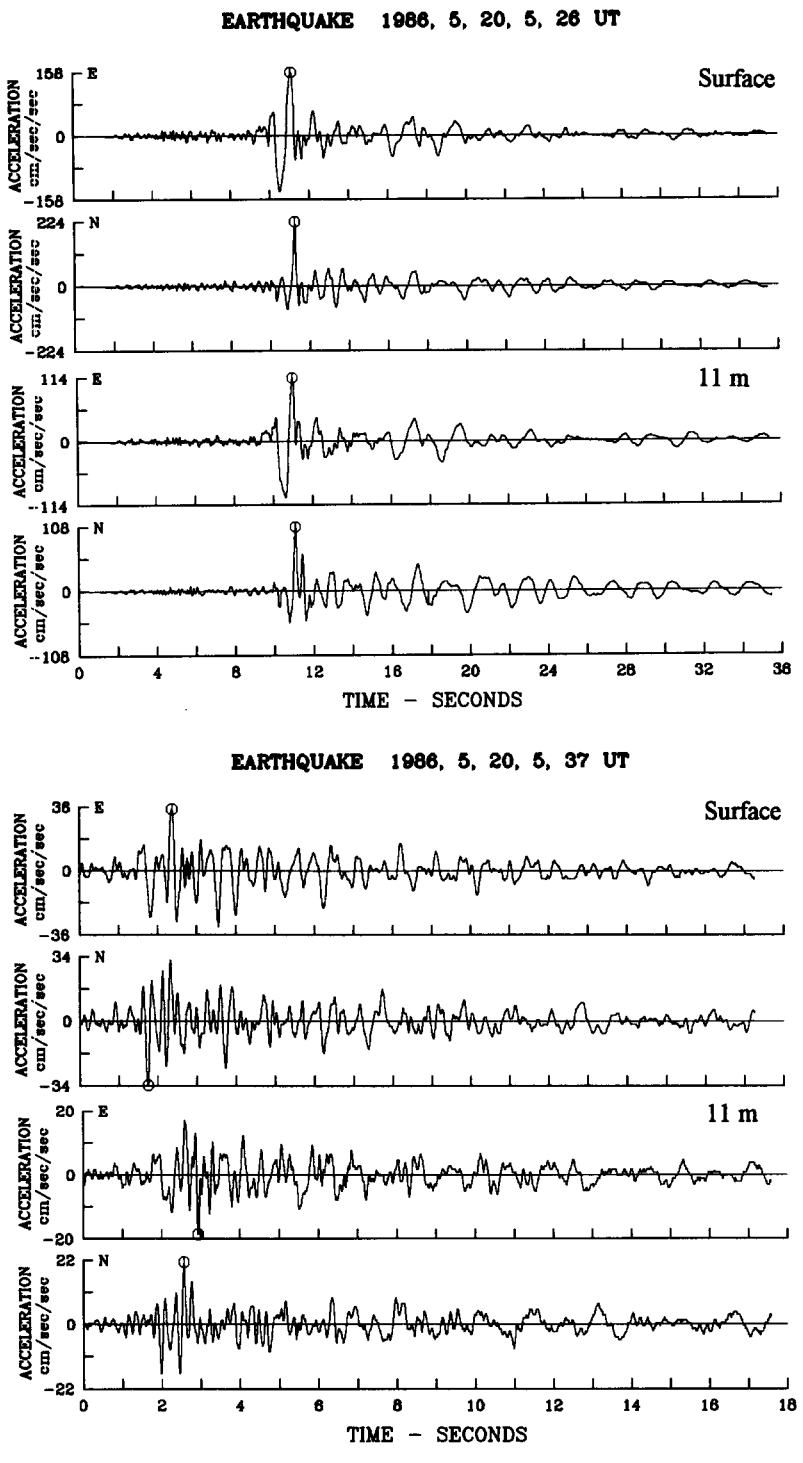

Fig. 9. Uphole/downhole accelerograms of the earthquakes of 20 May 1986 for which spectral ratios in Fig. 8(b) are calculated.

ratios of accelerations between the surface and the centre of a sedimentary stratum overlying bedrock, in cases where the deformation is assumed to be linear elastic and hysteretic. The layer in the model has a thickness of 20 m, and its shear wave velocity increases from about 100 to 320 m/s from the top to the bottom.

The theoretical nonlinear response does not come to a mere deamplification effect and can be separated into three characteristic frequency bands. Ratios are not affected by nonlinearity at the low frequencies since the wavelength becomes sufficiently long for the waves to ignore the layer. In the central frequency band, the deamplification in the nonlinear response occurs. Finally, strong motions are, conversely, amplified over weak motions in the high-frequency range owing to the effect of higher harmonics generation. The latter phenomenon is well known in the acoustics of intensive sound[36] and have been observed in the periodic seismic fields from the controllable sources[37,38] and the acoustic waves in rock;[39,40] it can be equally expected, albeit

never reported, in the strong earthquake-induced fields.

We verify the dissimilar behaviour of the uphole/downhole spectral ratios in the motions with different amplitude using borehole data from the LSST array. Figure 8(b) presents experimentally recorded spectral ratios obtained from the strong quake of 20 May 1986 and its aftershock (the same earthquake pair as used in Fig. 5, corresponding to events 7 and 8 in Table 3, see below) which caused peak horizontal accelerations at the surface of 224 and 35 cm/s^2, respectively. Original traces corresponding to the surface and 11-m accelerometers are shown in Fig. 9. Comparison of the curves in Figs 8(a) and (b) yields a good qualitative compliance. All three frequency bands in which linear and nonlinear responses differ in the theoretical prediction appear on the observed plots. Specifically, observed amplifications on weak and strong motion converge at the low-frequency limit. The central frequency band exists where the strong motion is deamplified compared with the weak motion. Ultimately, the over-amplification of the strong motion emerges above a cross-over frequency of approximately 10 Hz. Thus, observed data agree with the nonlinear site response characteristics anticipated from the hysteretic model of deformation.

An additional corollary is drawn from the analysis of Figs 5 and 7. They show that the soil amplification function derived from the coda supervening the main shear wave is a satisfactory approximation of the weak motion amplification. This indicates that the ground motion in coda is not affected by the foregoing substantially hysteretic behavior, so that the particle motion recurs to a linear regime a few seconds after its termination.

6 OBSERVED DEPENDENCE OF SHEAR WAVE VELOCITIES ON AMPLITUDE

Discussion connected with Fig. 1 has revealed that deamplification and shear wave velocity reduction effects exist in a couple. If one is observed, the other should be found concurrently.

We estimated effective shear wave velocity profiles at the LSST borehole for the earthquakes having variable peak acceleration stretching to 260 cm/s^2, using the radial horizontal component of acceleration. Velocities were calculated from the frequencies of the resonant peaks appearing in the spectral ratios of surface to four downhole accelerometers. To determine the location of resonant peaks, smoothed spectral ratios drawn on a linear scale were used. Details on applying the spectral ratio technique to the calculation of shear wave velocities and examples employing our data set are provided elsewhere.[41] Earthquake data used in these computations are given in Table 3.

The results are depicted in Fig. 10, where the circle size stands for the level of shaking at the ground surface, with the horizontal axis representing the deviation of the measured velocity from its low-strain value V_0 shown in Fig. 3. A clear dependence of the velocity on the acceleration amplitude is observed. It can be seen, first of all, that low-strain velocity profiles for different earthquakes in the acceleration range of 0–50 cm/s^2 do not coincide, their scattering indicating the error of velocity determination. Secondly, the deviation of the velocity from small-deformation value for the four large events with surface PGA exceeding 150 cm/s^2 is significantly larger than this error margin at the depths between 6 and 17 m, where the velocity is reduced by as much as 50%. Thus, the velocity reduction effect is well compatible with the amplitude-dependent amplification found in Fig. 8(b).

7 SUMMARY

A distinct nonlinear response of soils is found from the recordings of large earthquakes at two dense surface arrays and a vertical array in Taiwan. The data obtained are supportive of the hysteretic ground behaviour in the quakes with peak acceleration over 100–150 cm/s^2. However, these specific threshold accelerations cannot be regarded as strictly binding and may be soil-dependent. The possibility of their generalization will be clarified after the future investigations.

A postulate widely acknowledged in the state-of-the-art seismology has been that linear elasticity is able to account for the seismic phenomena even at strong motion levels, so that the ground response characteristics evaluated from the small-intensity earthquakes

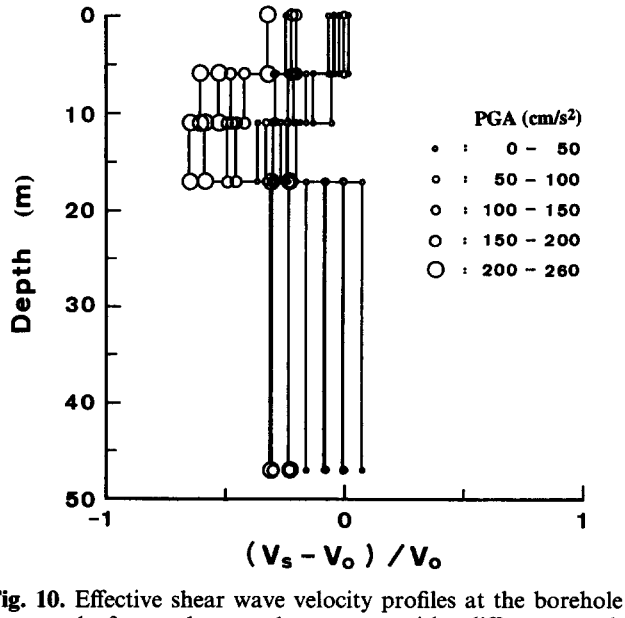

Fig. 10. Effective shear wave velocity profiles at the borehole measured from the accelerograms with different peak acceleration.

can be extrapolated directly to obtain the response at large earthquakes. This presumption is a basis of microzonation methods in which ground motions in large earthquakes are prognosticated. The latest experience shows that this practice may be misleading and that seismologists may have to consider the consequences of nonlinear ground behavior during earthquakes.

ACKNOWLEDGEMENTS

Permission by Taiwan Power Company (Republic of China) and the Electric Power Research Institute (USA) to use the unreleased data of the LSST array is gratefully acknowledged. We thank Dr H.-C. Chiu and the technical staff of the Institute of Earth Sciences of the Academia Sinica who are in charge of the operation of the SMART2 array. Corrected accelerograms were prepared by W. G. Huang and the data processing group. We are indebted to two reviewers whose constructive comments improved the quality of presentation. This work was supported by the National Science Council, Republic of China under the grant NSC 83-0202-M-001-004.

REFERENCES

1. Kanai, K., Takahasi, R. & Kawasumi, H. Seismic characteristics of ground. *Proc. WCEE*, Berkeley, CA, 1956, 31–1–16.
2. Gutenberg, B. Effects of ground on earthquake motion, *Bull. Seism. Soc. Am.*, 1957, **47,** 221–50.
3. Çelebi, M., Prince, J., Dietel, C., Onate, M. & Chavez, G. The culprit in Mexico City — amplification of motions, *Earthquake Spectra*, 1987, **3,** 315–28.
4. Seed, H. B., Romo, M. P., Sun, J. I., Jaime, A. & Lysmer, J. The Mexico Earthquake of September 19, 1985 — relationships between soil conditions and earthquake ground motions, *Earthquake Spectra*, 1988, **4,** 687–729.
5. Borcherdt, R. D. & Glassmoyer, G. On the characteristics of local geology and their influence on ground motions generated by the Loma Prieta Earthquake in the San Francisco Bay region, California, *Bull. Seism. Soc. Am.*, 1992, **82,** 603–41.
6. Boore, D. M. Stochastic simulation of high-frequency ground motions based on seismological models of the radiated spectra, *Bull. Seism. Soc. Am.*, 1983, **73,** 1865–94.
7. Papageorgiou, A. S. & Aki, K. A specific barrier model for the quantitative description of inhomogeneous faulting and the prediction of strong motion. Part I. Description of the model, *Bull. Seism. Soc. Am.*, 1983, **73,** 693–722.
8. Aki, K. Local site effect on ground motion. In *Earthquake Engineering and Soil Dynamics. II: Recent Advances in Ground-Motion Evaluation*, ed. J. L. Von Thun, ASCE Geotechnical Special Publication 20, 1988, pp. 103–55.
9. Phillips, W. S. & Aki, K. Site amplification of coda waves from local earthquakes in Central California, *Bull. Seism. Soc. Am.*, 1986, **76,** 627–48.
10. Finn, W. D. L. Geotechnical engineering aspects of microzonation. *Proc. 4th Int. Conf. on Seismic Zonation*, Vol. 1. Stanford, CA, 1991, 199–259.
11. Idriss, I. M. & Seed, H. B. An analysis of ground motions during the 1957 San Francisco earthquake, *Bull. Seism. Soc. Am.*, 1968, **58,** 2013–32.
12. Joyner, W. B. & Chen, A. T. F. Calculation of nonlinear ground response in earthquakes, *Bull. Seism. Soc. Am.*, 1975, **65,** 1315–36.
13. Lam, I., Tsai, C.-F. & Martin, G. F. Determination of site dependent spectra using non linear analysis, *Proc. 2nd Int. Conf. of Microzonation*, Vol. 2. San Francisco, CA, 1978, 1089–104.
14. Iwasaki, T., Kawashima, K. & Tatsuoka, F. Nonlinear seismic response analysis of soft soil deposits, *Proc. 7th Eur. Conf. on Earthquake Engineering*, Athens, Greece, 1982.
15. Erdik, M. Site response analysis. In *Strong Ground Motion Seismology*, ed. M. O. Erdik & M. N. Toksöz, D. Reidel Publishing Company, Holland, 1987, pp. 479–534.
16. Finn, W. D. L. Dynamic analysis in geotechnical engineering. In *Earthquake Engineering and Soil Dynamics. II: Recent Advances in Ground-Motion Evaluation*, ed. J. L. Von Thun. ASCE Geotechnical Special Publication 20, 1988, pp. 523–91.
17. Aki, K. & Irikura, K. Characterization and mapping of earthquake shaking for seismic zonation, *Proc. 4th Int. Conf. on Seismic Zonation*, Vol. 1. Stanford, CA, 1991, 61–110.
18. Chin, B.-H. & Aki, K. Simultaneous study of the source, path, and site effects on strong ground motion during the 1989 Loma Prieta Earthquake: a preliminary result on pervasive nonlinear site effects, *Bull. Seism. Soc. Am.*, 1991, **81,** 1859–84.
19. Yu, G., Anderson, J. G. & Siddharthan, R. On the characteristics of nonlinear soil response, *Bull. Seism. Soc. Am.*, 1993, **83,** 218–44.
20. Aki, K. Local site effects on weak and strong ground motions, *Tectonophysics*, 1993, **218,** 93–111.
21. Seed, H. B., Murarka, R., Lysmer, J. & Idriss, I. M. Relationships of maximum acceleration, maximum velocity, distance from source, and local site conditions for moderately strong earthquakes, *Bull. Seism. Soc. Am.*, 1976, **66,** 1323–42.
22. Sugito, M. & Kameda, H. Nonlinear soil amplification model with verification by vertical strong motion array records. *Proc. 4th U.S. Nat. Conf. on Earthquake Engineering*, Vol. 1. Palm Springs, CA, 1990, 555–64.
23. Abrahamson, N. A., Bolt, B. A., Darragh, R. B., Penzien, J. & Tsai, Y. B. The SMART1 accelerograph array (1980–1987), a review, *Earthquake spectra*, 1987, **3,** 263–87.
24. Beresnev, I. A., Wen, K.-L. & Yeh, Y. T. Source, path and site effects on dominant frequency and spatial variation of strong ground motion recorded by SMART1 and SMART2 arrays in Taiwan, *Earth. Eng. Struct. Dyn.*, 1994, **23,** 583–97.
25. Hardin, B. O. & Drnevich, V. P. Shear modulus and damping in soil: design equations and curves, *J. Soil Mech. Foundations Div. ASCE*, 1972, **98,** 667–92.
26. Mohammadioun, B. & Pecker, A. Low-frequency transfer of seismic energy by superficial soil deposits and soft rocks, *Earth. Eng. Struct. Dyn.*, 1984, **12,** 537–64.
27. Tokimatsu, K. & Midorikawa, S. Nonlinear soil properties estimated from strong motion accelerograms, *Proc. Int. Conf. on Recent Advances in Geotechnical Earthquake Engineering and Soil Dynamics*, Vol. 1. St. Louis, MO, 1981, 117–22.
28. Chang, C.-Y., Power, M. S., Tang, Y. K. & Mok, C. M. Evidence of nonlinear soil response during a moderate earthquake, *Proc. 12th Int. Conf. on Soil Mechanics and Foundation Engineering*, Vol. 3. Rio de Janeiro, 1989, 1–4.

29. Jarpe, S. P., Cramer, C. H., Tucker, B. E. & Shakal, A. F. A comparison of observations of ground response to weak and strong ground motion at Coalinga, California, *Bull. Seism. Soc. Am.*, 1988, **78,** 421–35.
30. Singh, S. K., Lermo, J., Dominguez, T., Ordaz, M., Espinosa, J. M., Mena, E. & Quaas, R. The Mexico earthquake of September 19, 1985 — a study of amplification of seismic waves in the Valley of Mexico with respect to a hill zone site, *Earthquake Spectra*, 1988, **4,** 653–73.
31. Singh, S. K., Mena, E. & Castro, R. Some aspects of source characteristics of the 19 September 1985 Michoacan earthquake and ground motion amplification in and near Mexico City from strong motion data, *Bull. Seism. Soc. Am.*, 1988, **78,** 451–77.
32. Darragh, R. B. & Shakal, A. F. The site response of two rock and soil station pairs to strong and weak ground motion, *Bull. Seism. Soc. Am.*, 1991, **81,** 1885–99.
33. Peng, H.-Y. & Wen, K.-L. Downhole instrument orientations and near surface Q analysis from the SMART2 array data, *Terrestrial, Atmospheric and Oceanic Sciences* (*Taiwan*), 1993, **4,** 367–80.
34. Wang, J.-H. Q values of Taiwan: a review, *J. Geol. Soc. China*, 1993, **36,** 15–24.
35. Lee, M. K. W. & Finn, W. D. L. DESRA-2, dynamic effective stress response analysis of soil deposits with energy transmitting boundary including assessment of liquefaction potential, *Soil Mechanics Series No. 38*, Dept. of Civil Engineering, University of British Columbia, Vancouver, 1978.
36. Zarembo, L. K. & Krasil'nikov, V. A. Nonlinear phenomena in the propagation of elastic waves in solids, *Soviet Phys. Uspekhi*, 1970, **13,** 778–97.
37. Beresnev, I. A., Nikolayev, A. V. Solov'yev, V. S. & Shalashov, G. M. Nonlinear phenomena in seismic surveying using periodic vibrosignals, *Izvestiya Academy of Sciences, USSR, Fizika Zemli* (*Physics of the Solid Earth*), 1986, **22,** 804–11.
38. Beresnev, I. A. & Nikolaev, A. V. Experimental investigations of nonlinear seismic effects, *Phys. Earth Planet. Inter.*, 1988, **50,** 83–7.
39. Meegan, G. D., Jr, Johnson, P. A., Guyer, R. A. & McCall, K. R. Observations of nonlinear elastic wave behavior in sandstone, *J. Acoust. Soc. Am.*, 1993, **94,** 3387–91.
40. Johnson, P. A. & McCall, K. R. Observation and implications of nonlinear elastic wave response in rock, *Geoph. Res. Letters*, 1994, **21,** 165–68.
41. Wen, K.-L. Nonlinear soil response in ground motions, *Earth. Eng. Struct. Dyn.*, 1994, **23,** 599–608.